

1

2

3

4

5

6

7 This is a preprint, and may be subject to further revisions.
8 Please note that subsequent versions of this manuscript may
9 have different content.

10

11

12 **Volcanic hazard exacerbated by future global warming–driven increase**
13 **in heavy rainfall.**

14 **Jamie I. Farquharson,¹ Falk Amelung,¹**

15 ¹ Rosenstiel School of Marine and Atmospheric Science, University of Miami, Miami,
16 FL, USA.

17 Corresponding author: Jamie I. Farquharson: jifarq89@googlemail.com

18 **Key Points:**

- 19 • Extreme rainfall is projected to increase in the majority of Earth's volcanic areas
20 • Extreme rainfall can lead to exacerbation of volcanic hazard, including dome
21 explosions, lahar generation, and flank collapse
22

23 **Keywords:** Climate change; Volcanism; GCM; Precipitation; Geosphere–Hydrosphere
24 interaction.

25 **Abstract**

26 Heavy rainfall drives a range of eruptive and noneruptive volcanic hazards; over the
27 Holocene, the incidence of many such hazards has increased due to rapid climate change.
28 Here we show that extreme heavy rainfall is projected to increase with continued global
29 warming throughout the 21st century in most subaerial volcanic regions, dramatically
30 increasing the potential for rainfall-induced volcanic hazards. This result is based on a
31 comparative analysis of nine general circulation models, and is prevalent across a wide
32 range of spatial scales, from countries and volcanic arcs down to individual volcanic
33 systems. Our results suggest that if global warming continues unchecked, the incidence
34 of primary and secondary rainfall-related volcanic activity—such as dome explosions or
35 flank collapse—will increase at more than 700 volcanoes around the globe. Improved
36 coupling between scientific observations—in particular, of local and regional
37 precipitation—and policy decisions, may go some way towards mitigating the increased
38 risk throughout the next 80 years.

39 **Plain-language Summary**

40 Extreme rainfall drives or worsens numerous volcanic hazards, including catastrophic
41 debris flows, flank failure events, and explosive eruptions. This is a poorly studied
42 phenomenon, with little research into its future evolution and implications. By analyzing
43 data from a suite of large climate models, we identify volcanic regions and even
44 individual volcanic systems where extreme rainfall is projected to increase over the next
45 century. We find that climate change–driven increase in extreme rainfall is linked to an
46 increased potential for multiple volcanic hazards—such as dome explosions or flank

47 collapse—at over 700 volcanoes. In light of as much as 2 °C committed global warming,
48 these results point to significant attendant implications for rainfall-related hazards at most
49 of Earth's subaerial volcanic systems within the foreseeable future.

50 **1. Climate change and volcanism**

51 The role of Earth's subaerial volcanism in driving past climate changes has been
52 substantial (Brönnimann et al., 2019)—due in large part to the radiative and chemical
53 effects of erupted gases and aerosols (Robock, 2000)—and it is anticipated to drive
54 further variability in the future (Bethke et al., 2017; Hyde & Crowley, 2000). In turn,
55 variations in climate have also been posited to drive volcanic activity (Aubry et al., 2021;
56 Cooper et al., 2018; Liggins et al., 2010; Rampino et al., 1979). Mechanisms such as the
57 isostatic unloading of the crust due to warming-induced glacial retreat and ice cap melt
58 (Albino et al., 2010; Swindles et al., 2017) or crustal stress changes generated by
59 changing sea levels (Bay et al., 2004) have been proposed to promote volcanic activity
60 over a range of spatio-temporal scales. Over the last 30 ka, changes in climate have
61 driven an increase in massive volcanic collapses, partly in response to increased humidity
62 and rainfall (Capra, 2006). An uptick in rainfall-driven volcanic hazards has been
63 proposed for many volcanic regions as global climate continues to warm throughout the
64 Anthropocene; in particular, in unglaciated high-relief volcanic environments (Liggins et
65 al., 2010): an observable rate change in hazardous geological phenomena that may
66 already be underway (McGuire, 2010).

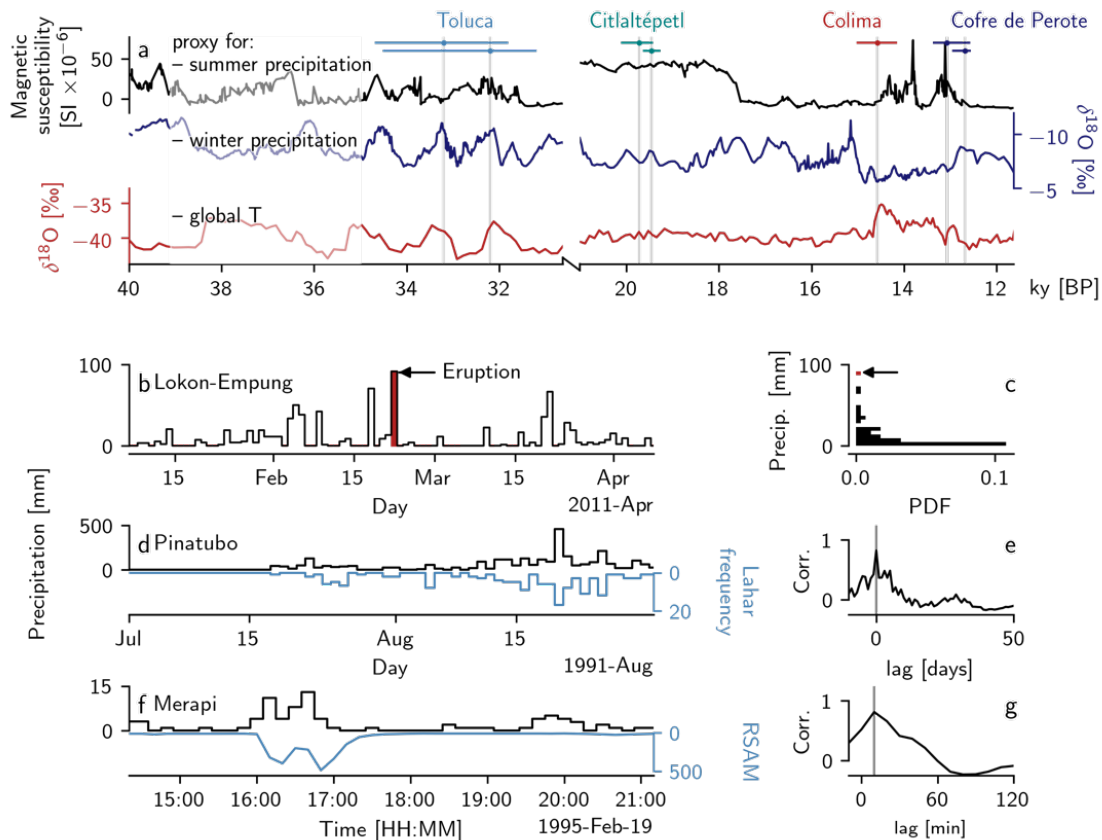
67

68 Extreme or seasonal rainfall has been identified as a trigger mechanism for primary
69 volcanic activity—discrete eruptions of lava, tephra, and gases—at multiple volcanoes.
70 Examples include rainfall-triggered explosions at Mount St Helens (USA), Gunung
71 Merapi (Indonesia), and Las Pilas (Nicaragua) (Mastin, 1994; Voight et al., 2000;
72 McBirney, 1955). Coupling between extreme rainfall events and dome collapse has also
73 frequently been noted (Barclay et al., 2006; Carn et al., 2004; Hicks et al., 2010;
74 Matthews et al., 2002; Matthews & Barclay, 2004), with heavy rainfall also being linked
75 to the generation of pyroclastic density currents (Barclay et al., 2006). More recently, a
76 link between extreme rainfall, pore fluid changes at depth, and magma propagation has
77 been proposed at Kīlauea Volcano, USA (Farquharson & Amelung, 2020). Rainfall-
78 triggered volcanism is often violently explosive (Mastin, 1994), and multiple direct
79 fatalities have been recorded as a result, including at Karkar (McKee et al., 1981),
80 Guagua Pichincha (Global Volcanism Program, 1993), and Karangetang (Global
81 Volcanism Program, 2011a) volcanoes (Papua New Guinea, Ecuador, and Indonesia,
82 respectively). Many hazards associated with extreme precipitation events or prolonged
83 rainfall are heightened in volcanic regions: not only do mountainous regions tend to
84 modify and amplify precipitation (Lagmay et al., 2015), but they are often mantled by
85 variably consolidated tephra deposits and other easily mobilized debris, and can be
86 associated with large thermal gradients. These gradients drive explosive fuel-coolant
87 interactions (Németh & Kósik, 2020), and thermal atmospheric forcing due volcanic
88 thermal anomalies can also increase precipitation above the threshold required to trigger
89 hazards (Poulidis et al., 2016). These factors promote a range of rainfall-related
90 secondary volcanic hazards, including the remobilization of volcanogenic deposits in the

91 form of lahars (Baumann et al., 2019; Kataoka et al., 2018; Paguican et al., 2009) and the
92 instigation of flank mass movement (Ayonghe et al., 2004; Eichenberger et al., 2013;
93 Marques et al., 2008; Towhata et al., 2021), a phenomenon that can in turn unload the
94 magma chamber and promote explosive decompression or dyke initiation (Manconi et al.,
95 2009). Volcanic slopes, typically with low cohesion and narrow grain-size distributions,
96 may be particularly disposed to mass wasting events (Eichenberger et al., 2013).

97
98 The timing, distribution, and amount of rainfall received by active volcanic systems is
99 influential over a range of timescales. **Figure 1a** indicates catastrophic Pleistocene sector
100 collapses of four volcanoes in Mexico: Volcán de Colima, Nevado de Toluca,
101 Citlaltépetl, and Cofre de Perote. In all cases, depositional sequences show evidence of
102 water saturation, hydrothermal alteration, and/or water circulation within the pre- and
103 syn-collapse edifice. In light of the lack of systematic concomitant magmatic activity,
104 pluvial conditions have instead been proposed to have triggered these volcanic collapses
105 (Capra et al., 2013). Tellingly, each of the events are associated with timeframes
106 characterized by locally high precipitation, typically concurrent with elevated global
107 temperatures. Similar climatic forcing of volcanic collapse has been identified for
108 volcanoes in Europe (Deeming et al., 2010) and South America (Tormey, 2010). Links
109 also exist over shorter timescales: at Lokon-Empung, a triggered volcanic eruption (22
110 February 2011) coincided with the quarterly rainfall maximum (**Fig. 1b,c**). **Figure 1d**
111 illustrates the intimate correlation between elevated rainfall and lahar generation (i.e. the
112 propagation of potentially devastating pyroclastic slurries) at Mt Pinatubo (Philippines),
113 with a lag of less than one day (**Fig. 1e**). Finally, **Fig. 1f** shows the hours-to-minutes
114 lahar response (reflected in Real-time Seismic-Amplitude Measurement: RSAM) at
115 Merapi. For both Pinatubo and Merapi, cross-correlation analysis reveals that lahar
116 occurrence is related to heavy rainfall with a sub-daily lag (as low as ten minutes in the
117 case of the latter: see **Fig. 1e,g**). Although **Fig. 1** highlights just a handful of volcanoes, a
118 textual analysis of the Smithsonian's Global Volcanism Program Bulletin Reports—a
119 multidecadal catalog of reports of volcanic activity—reveals that extreme or heavy
120 rainfall has been implicated in triggering or exacerbating hazards at at least 174 discrete

121 volcanoes: around 13 % or 1 in every 7 of Earth's subaerial volcanic inventory (see
 122 **Methods**).
 123



124 **Figure 1.** Extreme rainfall as a driver of volcanic hazards. **a** Pleistocene volcanic sector collapses
 125 of Volcán de Colima, Nevado de Toluca, Citlaltépetl, and Cofre de Perote (Mexico), reproduced
 126 after (Capra et al., 2013). Climate proxy data are described in the Methods. For each of the seven
 127 collapses, horizontal date ranges are indicated, as well as a vertical line highlighting the
 128 maximum probability collapse date. Note discontinuous x-axis. **b** The February 2011 eruption
 129 of Lokon-Empung is shown by a vertical line, alongside time-series of local precipitation data. **c**
 130 Lognormal distribution of precipitation data from **b**, with outlying value (corresponding to date
 131 of eruption) indicated. **d** Daily precipitation data (black) is plotted against the number of lahars
 132 per day (blue) observed at Pinatubo between July and September 1991. **e** Result of cross-
 133 correlation analysis of Pinatubo data shown in **d**, shown as correlation coefficient ("Corr.")
 134 between daily precipitation and lahar frequency versus lag. **f** Precipitation in ten-minute bins at
 135 Merapi volcano, alongside the RSAM value at the same temporal resolution. RSAM maxima
 136 reflect peak lahar surges. **g** Result of cross-correlation analysis of Merapi data shown in **f**, shown
 137 as correlation coefficient between ten-minute precipitation and RSAM value versus lag. Refer to
 138 **Methods** for all data sources.
 139
 140

141

142

143 As the rate of global climate change continues to accelerate, it becomes ever more crucial
144 to develop a comprehensive understanding of the manifold interactions and feedbacks
145 between the atmosphere, cryosphere, and solid Earth: complexly interconnected
146 components of the Earth system. Here we focus on the role of heavy rainfall in volcanic
147 environments, and the evolution of rainfall rates over a multi-decadal timeframe induced
148 by the ongoing rapid changes in global climate. A key problem with identifying volcanic
149 regions at increasing risk has been the inherent uncertainty of climate modeling (Liggins
150 et al., 2010). While there is broad consensus as to the direction of mean global
151 precipitation change (Min et al., 2011; Tebaldi et al., 2006), global climate models
152 (general circulation models: GCMs)—even when initiated with the same parameters—do
153 not show general concurrence upon the magnitude or spatial distribution of precipitation
154 change, and observations of global mean precipitation changes are at often odds with
155 projected changes (Gu & Adler, 2015). Consistently, however, these models project an
156 increase in the intensity and frequency of heavy precipitation—that is, extreme
157 precipitation events—both on global and regional scales (Collins et al., 2013). Fischer et
158 al. (2014) and Pfahl et al. (2017) demonstrate that global climate models tend to concur
159 when considering future heavy precipitation. In particular, those authors found that most
160 models tested in their analysis agreed on the sign of change of the diurnal maximum
161 precipitation over time at any given location.

162

163 In this contribution, we analyze a suite of numerical global climate models to assess
164 which of Earth's subaerial volcanoes are projected to experience increases or decreases in
165 extreme rainfall, revealing several volcanic systems which we estimate will become more
166 susceptible to rainfall-induced hazards over the next 80 years. In particular we focus on
167 the forced model response (FMR), the percentage change of heavy precipitation for a
168 given unit of global warming, which serves as a proxy for the likelihood of extreme
169 rainfall events, calculated from nine Coupled Model Intercomparison Project Phase 5
170 (CMIP5) general circulation models (**Methods**).

171

172

173 2. Materials and Methods

174 2.1 Climate proxy and volcanic hazard data

175

176 **Figure 1a** is reproduced after Capra et al., (2013), using magnetic susceptibility data
177 from lake sediment core from Pete-Itzá, Guatemala (Hodell et al., 2008) (interpreted to
178 reflect changes in summer precipitation), speleothem calcite $\delta^{18}\text{O}$ data from central New
179 Mexico (Asmerom et al., 2010) (interpreted to reflect changes in winter precipitation),
180 and the Greenland Ice Sheet Project 2 $\delta^{18}\text{O}$ (Grootes et al., 1993) as a proxy for global
181 temperature. Precipitation data in **Figure 1b** from Stasiun Geofisika Winangun (lon, lat:
182 124.83890, 1.44340) were accessed from Indonesia's Meteorology, Climatology and
183 Geophysics Agency (Badan Meteorologi, Klimatologi, dan Geofisika: BMKG) data
184 retrieval portal (<https://www.bmkg.go.id/>). Daily data of **Figure 1d** are from Pierson et

185 al., (1996). Merapi rainfall and RSAM data (**Figure 1f**) were digitized from Lavigne et
 186 al., (2000).

187

188 2.2 Textual analysis of Bulletin Reports

189

190 Geolocation data for Earth's subaerial volcanoes are obtained from the Smithsonian's
 191 Global Volcanism Program (GVP) databases (Global Volcanism Program, 2013) using
 192 the GVP webservice interface. We concentrate on volcanic systems active in the
 193 Holocene (discounting volcanoes defined as primarily submarine or subglacial): 1234
 194 volcanoes. The prior association of any particular volcano with rainfall-related volcanic
 195 hazard was determined by programmatically querying the catalogue GVP Bulletin
 196 Reports for the (case-insensitive) string literals "lahar", "heavy rain", "rainfall-triggered",
 197 "rainfall-induced", and "extreme rainfall" (ignoring punctuation and capitalization). The
 198 crawled reports were then manually parsed to identify volcanoes with previous evidence
 199 for volcanic hazard caused or exacerbated by rainfall, and to remove reports where
 200 rainfall was mention in non-hazard contexts (for example, reports on the effect of rainfall
 201 on monitoring equipment or the volcanic system that do not constitute a clear hazard,
 202 geographical background descriptions, or observational and logistical difficulties
 203 associated with inclement weather). The remaining catalog refers specifically to hazards
 204 associated with heightened rainfall activity: steam explosions; the instigation of lahars
 205 and mudflows; column collapse and pyroclastic density current generation; landslides,
 206 rockfalls, and other mass wasting events; flooding due to crater lake overflow; and
 207 triggered primary volcanic activity.

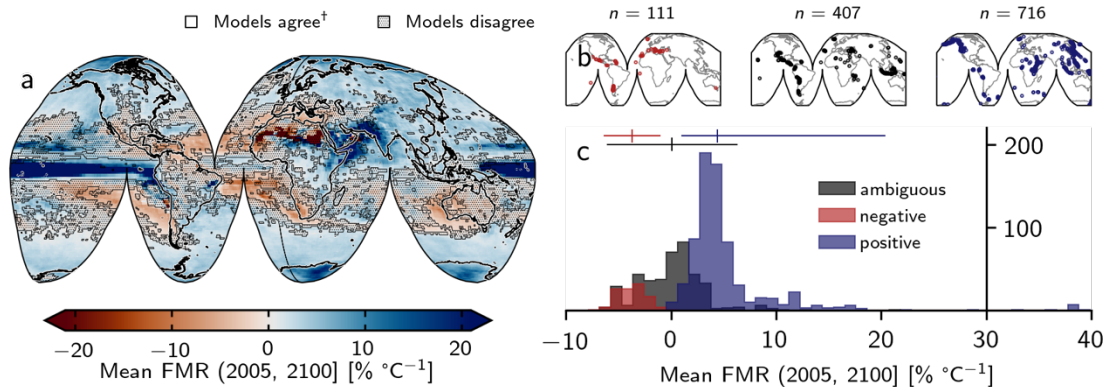
208

209 2.3 Forced model response

210

211 Ensemble climate projection experiment data were obtained from the Coupled Model
 212 Intercomparison Project Phase 5 (CMIP5). CMIP5 comprises a set of coordinated climate
 213 model experiments, performed by several independent modeling groups using more than
 214 50 discrete Earth System models, with the goal of providing a multi-model assessment of
 215 simulated climate change (and variability thereof) over timescales from decades to
 216 centuries. For a more comprehensive background to CMIP5, the reader is referred to
 217 Taylor et al., (2012). Here, we use data from nine separate models, listed in **Table S1**,
 218 each of which follow the Representative Concentration Pathway (RCP) 8.5 scenario (a
 219 "high emissions" scenario). The total period covered by the selected data is from 2005 or
 220 2006 to 2100. For comparability, we use models from ensemble r1i1p1 only (i.e. the
 221 initial conditions and the constitutive model physics are the same, and differences in
 222 simulations reflect internal inter-model variability), at a monthly frequency. For each
 223 model and each year over the modelled period, we calculate the mean global temperature
 224 $\langle T \rangle$ timeseries and the maximum monthly rainfall value RXm for each grid cell. The
 225 forced model response (FMR) is calculated as the slope of a linear regression of RXm
 226 versus $\langle T \rangle$ normalized to 01-Jan-2006 (**Fig. 2, Fig. S1**) or 01-Jan-2021 (**Fig. 3 and Fig.**
 227 **4**). The resulting 2D array A_k , where k is the number of the model, has dimensions
 228 dependent on the initial spatial resolution of the model experiments (**Table S1**). For each
 229 model k , the value of each cell at latitude i and longitude j is binarized such that $B_{ijk} =$

230 $H(A_{ijk})$ where $H(x)$ is the Heaviside function and the boolean units 0 and 1 thus denote
 231 negative and positive forced model responses, respectively. To determine areas where the
 232 majority of models agree on the sign of heavy precipitation change, we resample the
 233 binary arrays onto a common 180×360 grid (i.e. $\sim 1 \times 1^\circ$) using a nearest-neighbor
 234 approach, then sum them such that $C = \sum_{k=1}^{n=N} B_k$. Agreement in the sign of normalized
 235 RXm across at least seven of nine models is represented by $|C_{ij} - (9/2)| > 2$, where
 236 $C_{ij} \in [0,9]$. This criterion (7/9 models or 78 % model agreement) is comparable to the
 237 threshold imposed by previous studies (Fischer et al., 2014; Pfahl et al., 2017).
 238 Calculated forced model responses from the individual CMIP5 general circulation models
 239 are shown in **Fig. S1**.
 240



241 **Figure 2. Breakdown of mean forced model response.** **a** Global mean forced model response
 242 (FMR) calculated from all models. Shaded area indicates those regions where fewer than seven
 243 of nine models agreed on the sign of change (26.55 %). † at least seven of nine models agree on
 244 the sign of change. **b** Subaerial volcano geolocations separated according to whether models
 245 agree on a decrease in heavy precipitation with increased warming (red: “negative”; $n = 111$);
 246 the precipitation response is ambiguous due to lack of model agreement (black: “ambiguous”;
 247 $n = 407$); models agree on an increase in heavy precipitation with increased warming (blue:
 248 “positive”; $n = 716$). n indicates the number of discrete Holocene-active volcanic systems in each
 249 category. **c** Histogram of mean FMR for each group of volcanoes (as in **b**). Mean and two
 250 standard deviation range are indicated by the vertical and horizontal lines, respectively
 251 (**Methods**).
 252

253
 254

255 2.4 Distribution statistics and other calculations

256

257 Additional analyses were performed on an ad hoc basis for individual systems or sets; for
 258 completeness, these methods are described here. Where appropriate, volcano slope
 259 steepness was calculated using the database compiled by Grosse et al., (2013). Based on
 260 Shuttle Radar Topography Mission (SRTM) digital elevation data, Grosse et al., (2013)
 261 compute flank slopes for 50 m elevation intervals for 759 volcanoes. Maxima and mean
 262 slope values were calculated from this database. Uniformity was tested for using the chi-
 263 squared (χ^2) method. Statistical significance was ascribed where the cumulative
 264 distribution function of the chi-squared statistic CDF(χ^2) was less than 0.01. Descriptive

265 statistics of volcano FMR distributions (**Fig. 2c**) were calculated assuming a normal
 266 distribution (“negative” and “ambiguous”) and a log-normal distribution (“positive”).
 267 Cross-correlation analysis of Pinatubo and Merapi lahar data was performed by treating
 268 rainfall and lahar data as 1-dimensional sequences. **Figure 1e** and **1g** show the correlation
 269 coefficient for each lag value, in days (Pinatubo) or minutes (Merapi). Correlation
 270 maxima are 0 days and 10 minutes, respectively, indicating a relatively short lag between
 271 heavy rainfall and lahar occurrence at both sites.

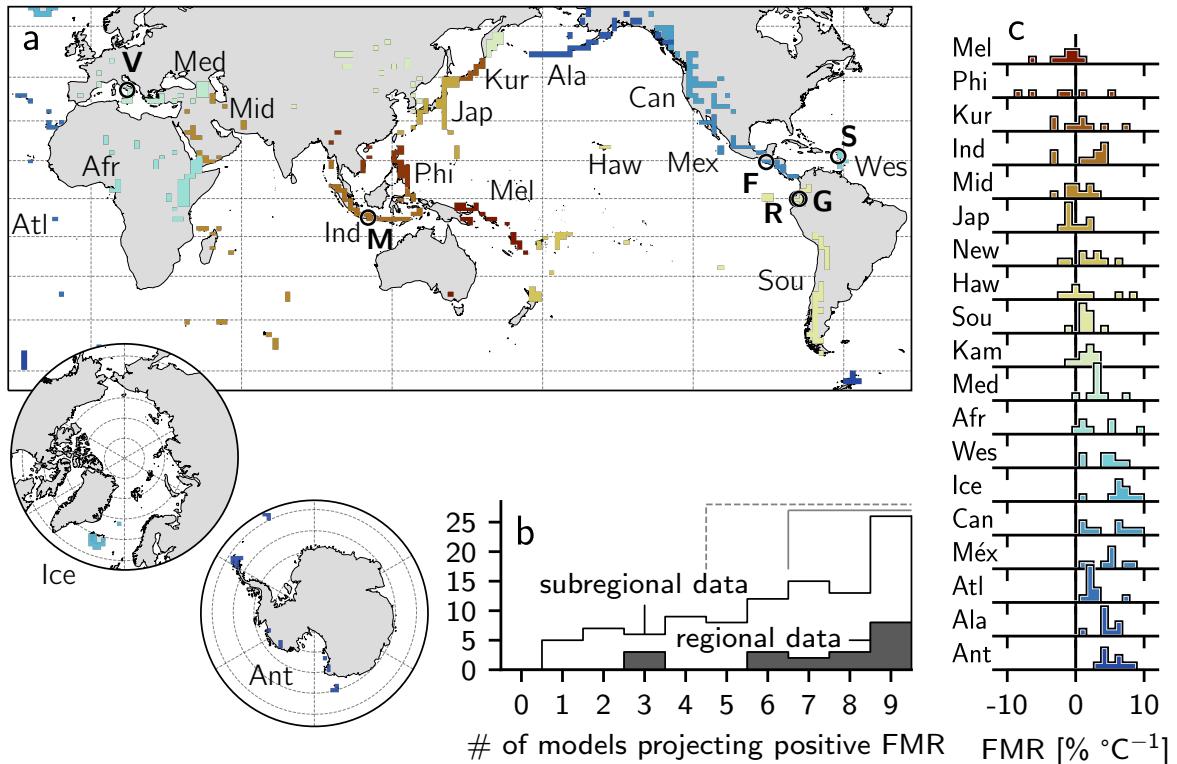
272

273 **3. Climate models agree on the direction of heavy precipitation change with** 274 **global warming**

275 Calculated forced model responses from the individual CMIP5 general circulation models
 276 are shown in **Fig. S1**, presented in $\% \text{C}^{-1}$ as the gradient of a regression between monthly
 277 heavy precipitation change RXm and global mean temperature $\langle T \rangle$. There is qualitative
 278 agreement in many areas across models: less extreme rainfall is forecast by most models
 279 for the majority of Australia, parts of Saharan and southern Africa, and Central America,
 280 for example, whereas large portions of North America, Eurasia, East Africa, and the Polar
 281 regions are projected to experience an increase in extreme precipitation with continued
 282 global warming. This is emphasized by mean response of all models resized onto a
 283 common grid (**Fig. 2a**). The areas where fewer than seven of nine models agree on the sign
 284 of FMR are shaded. The area over which at least seven of nine models concur accounts for
 285 73.45 % of the globe, in line with previous multi-model studies (Fischer et al., 2014; Pfahl
 286 et al., 2017), despite the fact that the cited studies examine models at a daily resolution
 287 over longer timescales (including historical simulations) and analyze more models (15 and
 288 22, respectively). As well as the proportion of model agreement, we highlight that the areas
 289 of agreement are qualitatively similar to those of Fischer et al., (2014) and Pfahl et al.,
 290 (2017). In a volcanic context, regions where extreme rainfall is projected to increase
 291 account for large portions of each of the continental volcanic arcs (the Cascades, the
 292 Alaskan Peninsula and Aleutian Range, Kamchatka, and Northern and Central Andes),
 293 parts of the Mediterranean and East African Rift system, and throughout the Sunda,
 294 Philippine, Ryuku, Japan, Kuril, Aleutian and West Indies island arcs. Smaller subtropical
 295 island arcs, including the Bismarck Archipelago are also encompassed. On the other hand,
 296 models tend to agree that extreme rainfall will decrease in parts of the Southern Andean
 297 Volcanic Zone and Rangitāhua (the Kermadec Islands), for example.

298 Of the 1234 Holocene-active subaerial volcanic systems included in the initial dataset, 768
 299 (59 %) are situated in regions with a positive FMR (i.e. regions that are forecast to
 300 experience more extreme rainfall over the next 80 years) across the majority of GCMs (**Fig.**
 301 **2b**). 244 of these (19 % of the initial dataset) have a mean (averaged over all models) FMR
 302 $\geq 5 \% \text{C}^{-1}$. Nineteen volcanoes (1.5 %) exhibit a mean FMR $\geq 20 \% \text{C}^{-1}$, all of which are
 303 located in the Galápagos, the East African Rift, and Papua New Guinea, between 3.125°S
 304 and 25.000°N . Highlighted in **Fig. 2b**, only 111 volcanoes (9 %) are located in regions
 305 anticipated to experience less extreme rainfall, with the remaining 407 (33 %) being
 306 associated with an ambiguous FMR (where fewer than 7 of the 9 models agreed with the
 307 sign of heavy precipitation change). We note that the proportion of volcanic systems
 308 associated with positive or negative FMR changes negligibly if the grid size is arbitrarily

309 reduced. The aggregate FMR distribution of each of the models is approximately
 310 symmetrical around a median of 3.2 % C⁻¹, indicating that the majority of the globe is
 311 projected to experience an increase in extreme rainfall. When we consider only those grid
 312 cells containing active volcanic systems (**Fig. 2C**), we observe a lognormal distribution of
 313 volcanoes with positive FMR, with a mean value of ~4.5 % C⁻¹ and a long tail on the
 314 positive side: the substantive majority of Earth's subaerial volcanic systems will be subject
 315 to more extreme rainfall with every increment of global warming over the remainder of the
 316 21st century.

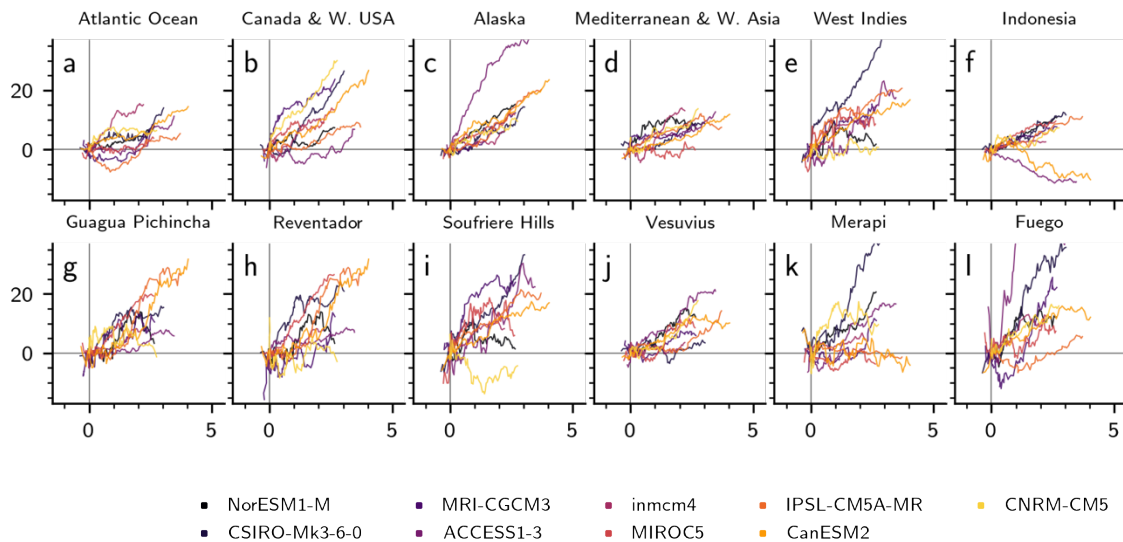


317 **Figure 3. Regional and sub-regional spatial averages.** **a** Map indicating the noncontiguous
 318 spatial extent over which regional data are averaged. Circle markers indicate individual
 319 volcanoes shown in Figure 4. V = Vesuvius, M = Merapi, F = Fuego, R = Reventador, G = Guagua
 320 Pichincha, S = Soufrière Hills Volcano. [Inset] polar regions. Regions are represented by discrete
 321 colored rectilinear polygons. Ant = Antarctica; Atl = Atlantic Ocean; Sou = South America; Ala =
 322 Alaska; Kur = Kuril Islands; Ind = Indonesia; Mid = Middle East and Indian Ocean; Phi = Philippines
 323 and SE Asia; Méx = México and Central America; Jap = Japan, Taiwan, and Marianas; Kam =
 324 Kamchatka and Mainland Asia; Med = Mediterranean and Western Asia; New = New Zealand to
 325 Fiji; Haw = Hawai'i and Pacific Ocean; Ice = Iceland and Arctic Ocean; Afr = Africa and Red Sea;
 326 Wes = West Indies; Mel = Melanesia and Australia; Can = Canada and Western USA. **b** Bar chart
 327 of the number of regions and subregions where x number of models project a spatially
 328 averaged forced model response (FMR) > 0 (i.e. a concomitant increase in heavy precipitation
 329 and global mean temperature). Dashed bracket indicates the majority of models, solid bracket
 330 indicates 7 or more out of 9 models. **c** Inter-model distributions of calculated FMR for each
 331 region. Marginal pie charts indicate the proportion of models that project a positive FMR per
 332 region (out of maximum of nine).

334
335
336
337
338
339
340
341
342
343
344
345

4. Models project an increase in heavy precipitation for most or all volcanic regions

The GVP subdivides Earth's volcanoes into 19 discrete regions, which are further subdivided into 101 subregions. Extracting areal averages of these volcanic regions (those grid cells containing at least one Holocene-active volcano: discrete colored rectilinear polygons in **Fig. 3a**), we calculate the linear regression-based gradient of change in heavy precipitation versus global warming. A summary of the results is given in **Table 1**.



346

347
348
349
350
351
352
353

Figure 4. Forced model responses at different spatial scales. a–f Percent change in modeled heavy rainfall per degree of global warming. Data are shown as a 30-yr rolling mean, normalised to January 2021. Data are areal averages (see **Figure 3** for areal extent of each region). **g–l** As **a–f**, for individual volcanic systems. Data correspond to the bounding pixel for each model (see **Methods**). Volcano locations are shown in **Figure 3**.

Table 1. Model analysis results. Abbreviation corresponds to the three-letter code on **Figure 3**. *n* is the number of historically active volcanoes within the region. Mean and median FMR values are given, along with standard deviation from the mean. “min” and “max” refer to the minimum and maximum calculated values of FMR for each region. “# +ve” refers to the number of models (out of nine) that yield a positive FMR value (see **Figure 3c**).

Region			FMR					
abbr.	name	<i>n</i>	mean	st. dev.	median	min	max	# +ve
Mel	Melanesia and Australia	66	-3.04	4.97	-0.98	-	1.16	3
						15.8		
						7		

Phi	Philippines and SE Asia	47	-3.02	7.58	-2.54	-	10.84	3
						13.4		
						1		
Kur	Kuril Islands	41	0.97	3.35	0.79	-3.57	7.78	6
Ind	Indonesia	125	1.68	2.72	2.92	-3.39	4.23	7
Mid	Middle East and Indian Ocean	41	0.49	1.93	0.50	-3.02	3.63	6
Jap	Japan, Taiwan, and Marianas	105	-0.08	1.28	-0.56	-2.28	2.24	3
New	New Zealand to Fiji	30	1.93	2.36	1.60	-1.73	6.18	7
Haw	Hawai'i and Pacific Ocean	6	4.56	8.18	1.18	-1.59	25.93	6
Sou	South America	182	1.67	1.45	1.48	-0.90	4.63	8
Kam	Kamchatka and Mainland Asia;	85	1.45	1.12	1.63	-0.54	3.03	8
Med	Mediterranean and Western Asia	38	3.09	1.87	2.90	-0.14	7.38	8
Afr	Africa and Red Sea	119	6.24	5.53	5.40	0.44	16.43	9
Wes	West Indies	15	5.01	2.85	5.12	0.61	10.94	9
Ice	Iceland and Arctic Ocean	27	6.55	2.36	6.81	0.69	9.48	9
Can	Canada and Western USA	64	5.16	2.92	6.06	0.87	9.21	9
Méx	México and Central America	109	5.72	3.11	5.58	0.99	12.02	9
Atl	Atlantic Ocean	23	2.78	1.72	2.27	1.23	7.44	9
Ala	Alaska	86	5.25	2.70	4.61	1.25	11.86	9
Ant	Antarctica	25	5.38	1.37	4.92	3.57	8.05	9

359

360

361 For each region, **Fig. 3b** indicates the distribution of models (out of a maximum of nine)
362 that project a positive FMR: a concomitant increase in heavy rainfall with global
363 warming. For the vast majority of volcanic regions (16/19: 84 %), most models project
364 positive FMR. Of these, 13 (64 %) exhibit agreement across at least seven models, and
365 for 8 regions (Antarctica; Atlantic Ocean; Alaska; Africa and Red Sea; México and
366 Central America; Iceland and Arctic Ocean; West Indies; Canada and Western USA) all
367 models forecast a positive FMR (42 % of all regions). There are zero volcanic regions for
368 which at least seven of nine models project a negative FMR. This trend is echoed at the
369 sub-regional scale (**Fig. 3b**): the majority of models forecast positive FMR for 74 of 101
370 subregions (73 %), and of these, 54 (53 %) exhibit agreement between at least seven
371 models. There are no volcanic regions for which more than seven models project a

372 negative FMR (c.f. inset pie charts of **Fig. 3c**). At both the region and subregion scale,
 373 the observed distributions are statistically nonuniform, characterized by $CDF(\chi^2) \ll 0.01$.
 374 **Fig. 3c** shows the distribution of calculated gradients across models for each region. Note
 375 that majority-positive FMR distributions (e.g. Antarctica, Alaska, Atlantic Ocean,
 376 Mediterranean and Western Asia, Kamchatka and Mainland Asia: **Fig. 3c**) tend to be
 377 relatively tightly clustered, whereas for those regions where FMR is predominantly
 378 negative or ambiguous (e.g. Philippines, Kuril Islands, Hawai'i and Pacific Ocean: **Fig.**
 379 **3c**), the distribution tends to be broader. The proportion of models exhibiting a positive
 380 FMR is indicated for each region by the marginal pie charts. We note that for eight
 381 regions, all models project a positive regional FMR (see also **Table 1**). Together, this
 382 emphasizes the fact that when we observe reasonable inter-model concurrence in any
 383 given region, the result is usually that heavy rainfall is set to increase over the next 80
 384 years.

385

386 Illustrative examples of regionally averaged climate projections are given in **Fig. 4a–f**,
 387 highlighted here due to the demonstrable risk of rainfall-induced hazard therein (data for
 388 all regions and subregions are provided in **Fig. S2**). The Atlantic ocean volcanic region
 389 (**Fig. 3a, Fig. 4a**) largely comprises island volcanoes characterized by a history of
 390 catastrophic collapse—including Tristan de Cunha, El Hierro, and Tenerife—a potential
 391 tsunamigenic hazard facilitated by wet climates (Hürlimann et al., 1999). The Canada and
 392 Western USA volcanic region (**Fig. 3a, Fig. 4b**) is predominantly composed of
 393 stratovolcanoes in the Cascade Range. The incidence of sector collapse at several
 394 Cascadian volcanoes (including Mount St Helens, Mt Adams, and Mt Baker) has been
 395 proposed to be triggered or exacerbated by historical climate change, including the
 396 attendant increase in humidity and rainfall (Capra, 2006). Numerous volcanoes in the
 397 Cascade Range currently present a significant lahar threat to major population centers
 398 (Hickson, 1994), with several exhibiting flank segments in excess of 20° slope pitch
 399 (calculated from Grosse et al., (2013)). Notably, direct evidence of rainfall-triggered
 400 explosive activity has been reported for Mount St Helens (Mastin, 1994). The Alaska
 401 region (**Fig. 3a, Fig. 4c**)—including the Alaskan Peninsula, Aleutian Range, and Aleutian
 402 island arc—hosts volcanoes with the highest mean and partial flank inclines (in excess of
 403 30 and 40°, respectively (calculated after Grosse et al., 2013)). Holocene climate change
 404 has already been shown to have driven geologically recent volcanic sector collapse in
 405 parts of the Mediterranean and Western Asia region (**Fig. 3a, Fig. 4d**) (Deeming et al.,
 406 2010), with these areas highlighted as becoming increasingly hazard-prone in the future
 407 (McGuire, 2010). The West Indies region (**Fig. 3a, Fig. 4e**) has similarly been
 408 highlighted (McGuire, 2010), and hosts frequently active volcanoes such as Soufrière
 409 Hills where primary volcanic activity is observably triggered by heavy rainfall (Barclay
 410 et al., 2006; Matthews et al., 2002). Finally, Indonesia (**Fig. 3a, Fig. 4f**)—the world's
 411 most volcanically active country and a volcanic region unto itself—is home to multiple
 412 volcanoes where explosive behavior has been triggered by heavy rainfall. Notable
 413 examples are provided by excerpts from Smithsonian Institution's Global Volcanism
 414 Program (GVP) Bulletin Reports:

415 *“This first Bulletin report discussing Egon describes the sudden appearance of*
 416 *volcanic activity there in January 2004. Heavy rains fell over Egon and its*

417 *surrounding area on 28 January ... followed at 1700 by an explosion and a black*
 418 *ash cloud rising ~ 750 m above the summit”* (Global Volcanism Program, 2004);

419 *“A sudden eruption at Karangetang on 6 August 2010 occurred without warning*
 420 *and caused considerable damage ... four people were confirmed dead and five were*
 421 *injured ... [An official noted] that the volcano erupted just after midnight when*
 422 *water from heavy rains had penetrated the volcano's hot lava dome, causing the*
 423 *explosion.”* (Global Volcanism Program, 2011a);

424 *“The phreatic eruption [of Lokon-Empung] was triggered by extensive rainfall;*
 425 *specifically, 602 mm of rain fell during January 2002 compared to 193 mm during*
 426 *December 2001. This excessive rainfall was thought to cause instability of the*
 427 *edifice.”* (Global Volcanism Program, 2002);

428 *“[O]n 22 February 2011, a phreatic eruption [of Lokon-Empung] ... was possibly*
 429 *triggered by high rainfall”* (Global Volcanism Program, 2011c).

430

431 Clearly, each of these volcanic regions appears particularly hazard-prone in terms of
 432 heavy rainfall-driven phenomena. Just as clearly, heavy rainfall is projected to increase
 433 in these regions by most or all climate models, thus heightening an already considerable
 434 threat to life, property, and infrastructure in the coming decades.

435

436 **5. Climate change—induced hazards at individual volcanoes**

437

438 **Figure 4g–l** presents the forced model responses at the scale of individual volcanic
 439 systems: Guagua Pichincha and Reventador, Ecuador; Soufrière Hills Volcano,
 440 Montserrat; Vesuvius, Italy; Gunung Merapi, Indonesia; and Fuego (Chi Q'aq'),
 441 Guatemala. These six volcanoes are chosen due to particularities of their eruptive
 442 histories, each of which illustrates the potential for increased hazard in the face of
 443 increased heavy precipitation. At Guagua Pichincha (**Fig. 3a, Fig. 4g**), cycles of
 444 explosivity have been anecdotally attributed to the timing of the rainy season (Global
 445 Volcanism Program, 1993). A violent explosive eruption in 1993, triggered by
 446 “abnormally high” rainfall, resulted in the death of two volcanologists. Reventador (**Fig.**
 447 **3a, Fig. 4h**), one of the most active volcanoes in Ecuador, is situated in a cloud-forest
 448 region already characterized by extremely heavy rainfall. Combined with its steep slopes
 449 (Grosse et al., 2013), these factors contribute to the generation of frequent, often
 450 destructive, lahars. An analysis of Reventador’s historical eruption catalogue indicates a
 451 tendency towards erupting between December and May (**Fig. S3a**), when the volcano
 452 receives the majority of its annual rainfall. Soufrière Hills Volcano (**Fig. 3a, Fig. 4i**) is
 453 characterized by sensitivity to heavy rainfall: not only does lahar probability scale
 454 directly with rainfall intensity (Jones et al., 2017), but triggered primary volcanic activity
 455 has been reported frequently (Barclay et al., 2006; Hicks et al., 2010; Matthews et al.,
 456 2002). At Vesuvius (**Fig. 3a, Fig. 4j**), textural, geochemical, and anecdotal evidence of
 457 external water—possibly of meteoric origin—exists for several previous large eruptions
 458 (Rolandi et al., 1993; Scandone et al., 1993). As with Reventador, we note a tendency for
 459 large historic eruptions to occur between July and December (the wettest time of year;

460 **Fig. S3b**). In 1998, a protracted period of extreme rainfall mobilized pyroclastic debris
461 from Vesuvius and the Campi Flegrei systems and generated devastating debris flows,
462 resulting in 160 fatalities with many more injured or displaced (Brondi & Salvatori,
463 2003). A statistical correlation between intense rainfall and explosive dome collapse has
464 been reported at Gunung Merapi (Voight et al., 2000) (**Fig. 3a, Fig. 4k**). The risk of
465 lahars at Merapi—invariably driven by rainfall (Lavigne et al., 2000)—is substantial,
466 with lahar deposits covering an area of almost 300 km² in the region. Rainfall-triggered
467 lahars at Merapi have been responsible for many deaths and the destruction of thousands
468 of homes. The 2010–2011 rainy season at Merapi was not only associated with a
469 cumulative rainfall amount more than 5 m greater than any year in the preceding decade
470 (fostered by a strong La Niña period), but also a substantially higher lahar frequency than
471 following previous eruptive events (as many as 59 in a single month (de Bélizal et al.,
472 2013)). Finally, at Fuego (**Fig. 3a, Fig. 4l**), heavy rainfall has been attributed to a host of
473 eruptive and non-eruptive hazards, triggering plume emissions, seismic activity, and tilt
474 changes (Global Volcanism Program, 1987), as well being directly related to frequently
475 triggered lahars. With climate models almost exclusively projecting an increase in heavy
476 precipitation with continued warming for each of these systems, it is highly probable that
477 the already substantial risk to people, property, and infrastructure at these systems will be
478 further amplified in the coming decades.

479

480

6. Perspectives

481

482 In summary, we find that the majority of Holocene-active subaerial volcanic systems
483 (716 volcanoes: 58 %) are confidently projected to experience more extreme rainfall as
484 global temperatures continue to rise. Moreover, in some volcanic areas, heavy
485 precipitation is projected to increase by as much as 46 % relative to the 2006 value for
486 every degree of warming experienced over the next 80 years. For another 33 % of
487 volcanoes globally (in particular at mid-latitudes), there is not sufficient inter-model
488 consensus to confidently estimate whether rainfall will become more or less extreme in
489 the future. Ultimately, these results point to significant attendant implications for rainfall-
490 related hazards at most of Earth's subaerial volcanic systems.

491

492 Multidecadal catalogues of reports of volcanic activity reveal that rainfall has historically
493 triggered, facilitated, or worsened primary volcanic activity or secondary hazards at over
494 170 subaerial volcanoes; a strong reminder that the influence of the hydrological cycle in
495 volcanic systems can be substantial (see also **Fig. 1**). This link emphasizes the
496 importance of considering rainfall in the development of hazard mitigation
497 strategies (Barclay et al., 2006; Jones et al., 2017; Pierson et al., 2014), and also
498 underscores the importance of developing novel instrumental monitoring systems
499 (Nagatani et al., 2018; Sanderson et al., 2018). The incorporation of meteorological data
500 into volcano monitoring systems has seen some limited adoption (Global Volcanism
501 Program, 2011b); nevertheless, meteorological data is far from being a standard
502 monitoring tool.

503

504 While much previous emphasis has been placed on the effect of climate change on
505 tropical volcanoes (McGuire, 2010), we highlight that an increase in heavy precipitation

506 is projected to occur with warming in many polar and temperate volcanic regions as well,
507 including the Aleutian Arc, Western USA and Canada, and Antarctica and the South
508 Sandwich Islands, as well as arid regions such as north Africa (**Fig. S2**). In resolving
509 cross-model agreement at regional and local scales relevant for volcanic hazard, we
510 demonstrate an explicit, geographically widespread link between global warming
511 scenarios and the potential for increased volcanic hazard. We have not accounted for the
512 influence of global warming on the dynamics of eruption plumes (Aubry 2016), nor for
513 the proposed orographic feedback between heated volcanic summits and precipitation
514 (Poulidis et al., 2017) which may serve to further exacerbate the influence of rainfall in
515 volcanic regions. Moreover, it is inevitable that the volcanic response to increasingly
516 extreme rainfall patterns will be strongly dependent on tectonic setting as a key
517 determinant of the nature of hazard exhibited at any given volcano: a level of complexity
518 that is not addressed here in detail. While previous studies have linked rainfall to
519 variations in eruptivity at basaltic shield volcanoes (Farquharson & Amelung, 2020;
520 Klein, 1984; Violette et al., 2001), the majority of quantitative evidence of rainfall-
521 induced volcanic hazard comes from intermediate, dome- and lahar-forming systems
522 such as Soufrière Hills Volcano (e.g. Matthews et al., 2002, 2009; Taron et al., 2007),
523 Gunung Merapi (de Bézizal et al., 2013; Voight et al., 2000), or Unzendake (Yamasato et
524 al., 1998). Further targeted research of the role of extreme rainfall in other settings (e.g.
525 continental rift zones) may provide invaluable context as to the sensitivity of individual
526 systems or volcanic regions. We highlight that broader feedback mechanisms have also
527 been proposed, including climate change–induced perturbations in crustal stress caused
528 by ice-sheet and glacier wastage (McGuire, 2010), changes to axial and spin-rate of the
529 Earth and realignment of the geoid (Anderson, 1974; Rampino et al., 1979), and rising
530 sea levels (McGuire et al., 1997), each of which have the potential to trigger subaerial
531 volcanism.

532

533 In focusing on extreme climate indices here, we do not quantify the absolute amount of
534 precipitation within the hydrogeological system at a given time. There is therefore
535 additional complexity involved in mechanisms which involve a threshold cumulative
536 amount of rainfall to enter the system, or rely on pre-existing system criticality.
537 Quantifying any climate change–induced increase in volcanic activity is nontrivial, and
538 the geospheric response to global warming and an increase in heavy precipitation will
539 certainly be geographically variable (McGuire, 2010). Nevertheless, we may look to
540 Earth system responses to previous long- and short-term changes in climate (e.g. **Fig. 1a**)
541 to provide some insight into the future (Knight & Harrison, 2013) as a committed global
542 warming of 1.5–2 °C by 2100 appears inevitable (Zhou et al., 2021).

543

544

545 **Author Contributions:** Conceptualization: JIF, FA; Methodology: JIF; Investigation:
546 JIF; Visualization: JIF; Supervision: FA; Writing—original draft: JIF; Writing—review
547 & editing: JIF, FA.

548

549 **Competing Interest Statement:** Authors declare that they have no competing interests.

550

551 **Acknowledgments**

552

553 We thank the climate modelling groups listed in **Table S1** for generating and making
 554 publicly available their model data. We also thank the attendant data distribution centers
 555 and the World Climate Research Programme's Working Group on Coupled modelling,
 556 which is responsible for CMIP5. We also thank the Smithsonian Institution for
 557 developing and maintaining the Global Volcanism Program, from which data are openly
 558 available. We thank Indonesia's Meteorology, Climatology and Geophysics
 559 Agency (Badan Meteorologi, Klimatologi, dan Geofisika: BMKG) for making rainfall
 560 data publicly available. We thank Sharanya Majumdar, Hannah Derbyshire, Fabian
 561 Wadsworth, and the WHWN writing group for invaluable discussions. "vik" and "roma"
 562 colourmaps were created by Fabio Cramer (http://doi.org/10.5281/zenodo.1243862).
 563 This work was supported by funding from the NASA's Interdisciplinary Research in
 564 Earth Science (IDS) program (grant number 80NSSC17K0028 P00003).

565

566 **Data and materials availability**

567

568 All necessary data and code required are provided in the following GitHub repository:
 569 [https://github.com/jifarquharson/rainfall-in-volcanic-](https://github.com/jifarquharson/rainfall-in-volcanic-regions/tree/main/Projects/Climate_forcing)
 570 [regions/tree/main/Projects/Climate_forcing](https://github.com/jifarquharson/rainfall-in-volcanic-regions/tree/main/Projects/Climate_forcing). This includes links to relevant open access
 571 repositories from which data were accessed. Model output data have been obtained
 572 through Earth System Grid Federation servers, in particular the node hosted by the
 573 Lawrence Livermore National Laboratory (<https://esgf-node.llnl.gov/search/cmip5/>).
 574 Data generated in the present study are available at the following repository: TBC.

575

576

577

578 **References**

- 579 Albino, F., Pinel, V., & Sigmundsson, F. (2010). Influence of surface load variations on eruption
 580 likelihood: application to two Icelandic subglacial volcanoes, Grímsvötn and Katla.
 581 *Geophysical Journal International*, 181(3), 1510–1524. [https://doi.org/10.1111/j.1365-](https://doi.org/10.1111/j.1365-246X.2010.04603.x)
 582 [246X.2010.04603.x](https://doi.org/10.1111/j.1365-246X.2010.04603.x)
- 583 Anderson, D. L. (1974). Earthquakes and the Rotation of the Earth. *Science*, 186(4158), 49–50.
 584 <https://doi.org/10.1126/science.186.4158.49>
- 585 Asmerom, Y., Polyak, V. J., & Burns, S. J. (2010). Variable winter moisture in the southwestern
 586 United States linked to rapid glacial climate shifts. *Nature Geoscience*, 3(2), 114–117.
 587 <https://doi.org/10.1038/ngeo754>
- 588 Aubry, T. J., Farquharson, J. I., Rowell, C., Watt, S., Pinel, V., Beckett, F., et al. (2021). Impact
 589 of climate change on volcanic processes: current understanding and future challenges.
 590 Retrieved from <https://eartharxiv.org/repository/view/2752/>
- 591 Ayonghe, S. N., Ntasin, E. B., Samalang, P., & Suh, C. E. (2004). The June 27, 2001 landslide on
 592 volcanic cones in Limbe, Mount Cameroon, West Africa. *Journal of African Earth*
 593 *Sciences*, 39(3), 435–439. <https://doi.org/10.1016/j.jafrearsci.2004.07.022>

- 594 Barclay, J., Johnstone, J. E., & Matthews, A. J. (2006). Meteorological monitoring of an active
595 volcano: Implications for eruption prediction. *Journal of Volcanology and Geothermal*
596 *Research*, 150(4), 339–358. <https://doi.org/10.1016/j.jvolgeores.2005.07.020>
- 597 Baumann, V., Bonadonna, C., Cuomo, S., Moscariello, M., Biass, S., Pistolesi, M., & Gattuso, A.
598 (2019). Mapping the susceptibility of rain-triggered lahars at Vulcano island (Italy)
599 combining field characterization, geotechnical analysis, and numerical modelling.
600 *Natural Hazards and Earth System Sciences*, 19(11), 2421–2449.
601 <https://doi.org/10.5194/nhess-19-2421-2019>
- 602 Bay, R. C., Bramall, N., & Price, P. B. (2004). Bipolar correlation of volcanism with millennial
603 climate change. *Proceedings of the National Academy of Sciences*, 101(17), 6341–6345.
604 <https://doi.org/10.1073/pnas.0400323101>
- 605 de Bézizal, E., Lavigne, F., Hadmoko, D. S., Degeai, J.-P., Dipayana, G. A., Mutaqin, B. W., et al.
606 (2013). Rain-triggered lahars following the 2010 eruption of Merapi volcano, Indonesia:
607 A major risk. *Journal of Volcanology and Geothermal Research*, 261, 330–347.
608 <https://doi.org/10.1016/j.jvolgeores.2013.01.010>
- 609 Bethke, I., Outten, S., Otterå, O. H., Hawkins, E., Wagner, S., Sigl, M., & Thorne, P. (2017).
610 Potential volcanic impacts on future climate variability. *Nature Climate Change*, 7(11),
611 799–805. <https://doi.org/10.1038/nclimate3394>
- 612 Brondi, F., & Salvatori, L. (2003). The 5--6 May 1998 mudflows in Campania, Italy. In J. Hervás
613 (Ed.), *Lessons learnt from landslide disasters in Europe* (pp. 5--16).
- 614 Brönnimann, S., Franke, J., Nussbaumer, S. U., Zumbühl, H. J., Steiner, D., Trachsel, M., et al.
615 (2019). Last phase of the Little Ice Age forced by volcanic eruptions. *Nature Geoscience*,
616 12(8), 650–656. <https://doi.org/10.1038/s41561-019-0402-y>
- 617 Capra, L., Bernal, J. P., Carrasco-Núñez, G., & Roverato, M. (2013). Climatic fluctuations as a
618 significant contributing factor for volcanic collapses. Evidence from Mexico during the
619 Late Pleistocene. *Global and Planetary Change*, 100, 194–203.
620 <https://doi.org/10.1016/j.gloplacha.2012.10.017>
- 621 Capra, Lucia. (2006). Abrupt climatic changes as triggering mechanisms of massive volcanic
622 collapses. *Journal of Volcanology and Geothermal Research*, 155(3), 329–333.
623 <https://doi.org/10.1016/j.jvolgeores.2006.04.009>
- 624 Carn, S., Watts, R. B., Thompson, G., & Norton, G. E. (2004). Anatomy of a lava dome collapse:
625 the 20 March 2000 event at Soufrière Hills Volcano, Montserrat. *Journal of Volcanology*
626 *and Geothermal Research*, 131(3–4), 241–264. [https://doi.org/10.1016/S0377-](https://doi.org/10.1016/S0377-0273(03)00364-0)
627 [0273\(03\)00364-0](https://doi.org/10.1016/S0377-0273(03)00364-0)
- 628 Collins, M., AchutaRao, K., Ashok, K., Bhandari, S., Mitra, A. K., Prakash, S., et al. (2013).
629 Observational challenges in evaluating climate models. *Nature Climate Change*, 3(11),
630 940–941. <https://doi.org/10.1038/nclimate2012>
- 631 Cooper, C. L., Swindles, G. T., Savov, I. P., Schmidt, A., & Bacon, K. L. (2018). Evaluating the
632 relationship between climate change and volcanism. *Earth-Science Reviews*, 177, 238–
633 247. <https://doi.org/10.1016/j.earscirev.2017.11.009>
- 634 Deeming, K. R., McGuire, B., & Harrop, P. (2010). Climate forcing of volcano lateral collapse:
635 evidence from Mount Etna, Sicily. *Philosophical Transactions of the Royal Society A:*
636 *Mathematical, Physical and Engineering Sciences*, 368(1919), 2559–2577.
637 <https://doi.org/10.1098/rsta.2010.0054>
- 638 Eichenberger, J., Ferrari, A., & Laloui, L. (2013). Early warning thresholds for partially saturated
639 slopes in volcanic ashes. *Computers and Geotechnics*, 49, 79–89.
640 <https://doi.org/10.1016/j.compgeo.2012.11.002>
- 641 Farquharson, J. I., & Amelung, F. (2020). Extreme rainfall triggered the 2018 rift eruption at
642 Kīlauea Volcano. *Nature*, 580(7804), 491–495. [https://doi.org/10.1038/s41586-020-](https://doi.org/10.1038/s41586-020-2172-5)
643 [2172-5](https://doi.org/10.1038/s41586-020-2172-5)

- 644 Fischer, E. M., Sedláček, J., Hawkins, E., & Knutti, R. (2014). Models agree on forced response
 645 pattern of precipitation and temperature extremes. *Geophysical Research Letters*, *41*(23),
 646 8554–8562. <https://doi.org/10.1002/2014GL062018>
- 647 Global Volcanism Program. (1987). Report on Fuego (Guatemala). *Scientific Event Alert Network*
 648 *Bulletin*, *12*(7). <https://doi.org/10.5479/si.GVP.SEAN198707-342090>
- 649 Global Volcanism Program. (1993). Report on Guagua Pichincha (Ecuador). *Bulletin of the*
 650 *Global Volcanism Network*, *18*(2). <https://doi.org/10.5479/si.GVP.BGVN199302-352020>
- 651 Global Volcanism Program. (2002). Report on Lokon-Empung (Indonesia). *Bulletin of the Global*
 652 *Volcanism Network*, *27*(2). <https://doi.org/10.5479/si.GVP.BGVN200202-266100>
- 653 Global Volcanism Program. (2004). Report on Egon (Indonesia). *Bulletin of the Global*
 654 *Volcanism Network*, *29*(3). <https://doi.org/10.5479/si.GVP.BGVN200403-264160>
- 655 Global Volcanism Program. (2011a). Report on Karangetang [Api Siau] (Indonesia). *Bulletin of*
 656 *the Global Volcanism Network*, *36*(1). [https://doi.org/10.5479/si.GVP.BGVN201102-](https://doi.org/10.5479/si.GVP.BGVN201102-267020)
 657 *267020*
- 658 Global Volcanism Program. (2011b). Report on Kirishimayama (Japan). *Bulletin of the Global*
 659 *Volcanism Network*, *36*(7). <https://doi.org/10.5479/si.GVP.BGVN201107-282090>
- 660 Global Volcanism Program. (2011c). Report on Lokon-Empung (Indonesia). *Bulletin of the*
 661 *Global Volcanism Network*, *36*(6). <https://doi.org/10.5479/si.GVP.BGVN201106-266100>
- 662 Global Volcanism Program. (2013). *Volcanoes of the World*, v. 4.9.1 (17 Sep 2020). Smithsonian
 663 Institution. Retrieved from <https://doi.org/10.5479/si.GVP.VOTW4-2013>
- 664 Grootes, P. M., Stuiver, M., White, J. W. C., Johnsen, S., & Jouzel, J. (1993). Comparison of
 665 oxygen isotope records from the GISP2 and GRIP Greenland ice cores. *Nature*,
 666 *366*(6455), 552–554. <https://doi.org/10.1038/366552a0>
- 667 Grosse, P., Euillades, P. A., Euillades, L. D., & van Wyk de Vries, B. (2013). A global database
 668 of composite volcano morphometry. *Bulletin of Volcanology*, *76*(1), 784.
 669 <https://doi.org/10.1007/s00445-013-0784-4>
- 670 Gu, G., & Adler, R. F. (2015). Spatial Patterns of Global Precipitation Change and Variability
 671 during 1901–2010. *Journal of Climate*, *28*(11), 4431–4453. [https://doi.org/10.1175/JCLI-](https://doi.org/10.1175/JCLI-D-14-00201.1)
 672 *D-14-00201.1*
- 673 Hicks, P. D., Matthews, A. J., & Cooker, M. J. (2010). Triggering of a volcanic dome collapse by
 674 rainwater infiltration. *Journal of Geophysical Research*, *115*(B9), B09212.
 675 <https://doi.org/10.1029/2009JB006831>
- 676 Hickson, C. (1994). Character of volcanism, volcanic hazards, and risk, northern end of the
 677 Cascade magmatic arc, British Columbia and Washington State. *Bulletin - Geological*
 678 *Survey of Canada*, *481*, 231–250.
- 679 Hodell, D. A., Anselmetti, F. S., Ariztegui, D., Brenner, M., Curtis, J. H., Gilli, A., et al. (2008).
 680 An 85-ka record of climate change in lowland Central America. *Quaternary Science*
 681 *Reviews*, *27*(11), 1152–1165. <https://doi.org/10.1016/j.quascirev.2008.02.008>
- 682 Hürlimann, M., Ledesma, A., & Martí, J. (1999). Conditions favouring catastrophic landslides on
 683 Tenerife (Canary Islands). *Terra Nova*, *11*(2–3), 106–111. [https://doi.org/10.1046/j.1365-](https://doi.org/10.1046/j.1365-3121.1999.00233.x)
 684 *3121.1999.00233.x*
- 685 Hyde, W. T., & Crowley, T. J. (2000). Probability of Future Climatically Significant Volcanic
 686 Eruptions. *Journal of Climate*, *13*(9), 1445–1450. [https://doi.org/10.1175/1520-](https://doi.org/10.1175/1520-0442(2000)013<1445:LOFCSV>2.0.CO;2)
 687 *0442(2000)013<1445:LOFCSV>2.0.CO;2*
- 688 Impact of global warming on the rise of volcanic plumes and implications for future volcanic
 689 aerosol forcing - Aubry - 2016 - Journal of Geophysical Research: Atmospheres - Wiley
 690 Online Library. (n.d.). Retrieved January 25, 2021, from
 691 <https://agupubs.onlinelibrary.wiley.com/doi/full/10.1002/2016JD025405>
- 692 Jones, R., Manville, V., Peakall, J., Froude, M. J., & Odbert, H. M. (2017). Real-time prediction
 693 of rain-triggered lahars: incorporating seasonality and catchment recovery. *Natural*

- 694 *Hazards and Earth System Sciences*, 17(12), 2301–2312. <https://doi.org/10.5194/nhess->
695 17-2301-2017
- 696 Kataoka, K. S., Matsumoto, T., Saito, T., Kawashima, K., Nagahashi, Y., Iyobe, T., et al. (2018).
697 Lahar characteristics as a function of triggering mechanism at a seasonally snow-clad
698 volcano: contrasting lahars following the 2014 phreatic eruption of Ontake Volcano,
699 Japan. *Earth, Planets and Space*, 70(1), 113. <https://doi.org/10.1186/s40623-018-0873-x>
- 700 Klein, F. W. (1984). Eruption forecasting at Kilauea Volcano, Hawaii. *Journal of Geophysical*
701 *Research: Solid Earth*, 89(B5), 3059–3073. <https://doi.org/10.1029/JB089iB05p03059>
- 702 Knight, J., & Harrison, S. (2013). The impacts of climate change on terrestrial Earth surface
703 systems. *Nature Climate Change*, 3(1), 24–29. <https://doi.org/10.1038/nclimate1660>
- 704 Lagmay, A. M. F., Bagtasa, G., Crisologo, I. A., Racoma, B. A. B., & David, C. P. C. (2015).
705 Volcanoes magnify Metro Manila's southwest monsoon rains and lethal floods. *Frontiers*
706 *in Earth Science*, 2. <https://doi.org/10.3389/feart.2014.00036>
- 707 Lavigne, F., Thouret, J. C., Voight, B., Suwa, H., & Sumaryono, A. (2000). Lahars at Merapi
708 volcano, Central Java: an overview. *Journal of Volcanology and Geothermal Research*,
709 100(1), 423–456. [https://doi.org/10.1016/S0377-0273\(00\)00150-5](https://doi.org/10.1016/S0377-0273(00)00150-5)
- 710 Liggins, F., Betts, R. A., & McGuire, B. (2010). Projected future climate changes in the context
711 of geological and geomorphological hazards. *Philosophical Transactions of the Royal*
712 *Society A: Mathematical, Physical and Engineering Sciences*, 368(1919), 2347–2367.
713 <https://doi.org/10.1098/rsta.2010.0072>
- 714 Manconi, A., Longpré, M.-A., Walter, T. R., Troll, V. R., & Hansteen, T. H. (2009). The effects
715 of flank collapses on volcano plumbing systems. *Geology*, 37(12), 1099–1102.
716 <https://doi.org/10.1130/G30104A.1>
- 717 Marques, R., Zêzere, J., Trigo, R., Gaspar, J., & Trigo, I. (2008). Rainfall patterns and critical
718 values associated with landslides in Povoação County (São Miguel Island, Azores):
719 relationships with the North Atlantic Oscillation. *Hydrological Processes*, 22(4), 478–
720 494. <https://doi.org/10.1002/hyp.6879>
- 721 Mastin, L. G. (1994). Explosive tephra emissions at Mount St. Helens, 1989–1991: The violent
722 escape of magmatic gas following storms? *GSA Bulletin*, 106(2), 175–185.
723 [https://doi.org/10.1130/0016-7606\(1994\)106<0175:ETEAMS>2.3.CO;2](https://doi.org/10.1130/0016-7606(1994)106<0175:ETEAMS>2.3.CO;2)
- 724 Matthews, A. J., & Barclay, J. (2004). A thermodynamical model for rainfall-triggered volcanic
725 dome collapse. *Geophysical Research Letters*, 31(5).
726 <https://doi.org/10.1029/2003GL019310>
- 727 Matthews, A. J., Barclay, J., Carn, S., Thompson, G., Alexander, J., Herd, R., & Williams, C.
728 (2002). Rainfall-induced volcanic activity on Montserrat. *Geophysical Research Letters*,
729 29(13), 22-1-22–4. <https://doi.org/10.1029/2002GL014863>
- 730 Matthews, A. J., Barclay, J., & Johnstone, J. E. (2009). The fast response of volcano-seismic
731 activity to intense precipitation: Triggering of primary volcanic activity by rainfall at
732 Soufrière Hills Volcano, Montserrat. *Journal of Volcanology and Geothermal Research*,
733 184(3–4), 405–415. <https://doi.org/10.1016/j.jvolgeores.2009.05.010>
- 734 McBirney, A. R. (1955). Thoughts on the eruption of the nicaraguan volcano las pilas. *Bulletin*
735 *Volcanologique*, 17(1), 113–117. <https://doi.org/10.1007/BF02596048>
- 736 McGuire, B. (2010). Potential for a hazardous geospheric response to projected future climate
737 changes. *Philosophical Transactions of the Royal Society A: Mathematical, Physical and*
738 *Engineering Sciences*, 368(1919), 2317–2345. <https://doi.org/10.1098/rsta.2010.0080>
- 739 McGuire, Bill. (2010). Climate forcing of geological and geomorphological hazards.
740 *Philosophical Transactions of the Royal Society A: Mathematical, Physical and*
741 *Engineering Sciences*, 368(1919), 2311–2315. <https://doi.org/10.1098/rsta.2010.0077>
- 742 McGuire, W. J., Howarth, R. J., Firth, C. R., Solow, A. R., Pullen, A. D., Saunders, S. J., et al.
743 (1997). Correlation between rate of sea-level change and frequency of explosive

- 744 volcanism in the Mediterranean. *Nature*, 389(6650), 473–476.
 745 <https://doi.org/10.1038/38998>
- 746 McKee, C. O., Wallace, D. A., Almond, R. A., & Talai, B. (1981). Fatal hydro-eruption of Karkar
 747 volcano in 1979: Development of a maar-like crater. *Cooke-Ravian Volume of*
 748 *Volcanological Papers, Geological Survey of Papua New Guinea*, 10, 63–84.
- 749 Min, S.-K., Zhang, X., Zwiers, F. W., & Hegerl, G. C. (2011). Human contribution to more-
 750 intense precipitation extremes. *Nature*, 470(7334), 378–381.
 751 <https://doi.org/10.1038/nature09763>
- 752 Nagatani, K., Kiribayashi, S., Yajima, R., Hada, Y., Izu, T., Zeniya, A., et al. (2018). Micro-
 753 unmanned aerial vehicle-based volcano observation system for debris flow evacuation
 754 warning. *Journal of Field Robotics*, 35(8), 1222–1241. <https://doi.org/10.1002/rob.21834>
- 755 Németh, K., & Kósik, S. (2020). Review of Explosive Hydrovolcanism. *Geosciences*, 10(2), 44.
 756 <https://doi.org/10.3390/geosciences10020044>
- 757 Paguican, E. M. R., Lagmay, A. M. F., Rodolfo, K. S., Rodolfo, R. S., Tengonciang, A. M. P.,
 758 Lopus, M. R., et al. (2009). Extreme rainfall-induced lahars and dike breaching, 30
 759 November 2006, Mayon Volcano, Philippines. *Bulletin of Volcanology*, 71(8), 845–857.
 760 <https://doi.org/10.1007/s00445-009-0268-8>
- 761 Pfahl, S., O’Gorman, P. A., & Fischer, E. M. (2017). Understanding the regional pattern of
 762 projected future changes in extreme precipitation. *Nature Climate Change*, 7(6), 423–
 763 427. <https://doi.org/10.1038/nclimate3287>
- 764 Pierson, T. C., Wood, N. J., & Driedger, C. L. (2014). Reducing risk from lahar hazards:
 765 concepts, case studies, and roles for scientists. *Journal of Applied Volcanology*, 3(1), 16.
 766 <https://doi.org/10.1186/s13617-014-0016-4>
- 767 Pierson, Thomas C., T., Daag, A. S., Delos Reyes, P. J., Regalado, Ma. T. M., Solidum, R. U., &
 768 Tubianosa, B. S. (1996). Flow and Deposition of Posteruption Hot Lahars on the East
 769 Side of Mount Pinatubo, July-October 1991. In *Fire and Mud: Eruptions and Lahars of*
 770 *Mount Pinatubo, Philippines*. Quezon City: Philippine Institute of Volcanology and
 771 Seismology.
- 772 Poulidis, A. P., Renfrew, I. A., & Matthews, A. J. (2016). Thermally Induced Convective
 773 Circulation and Precipitation over an Isolated Volcano. *Journal of the Atmospheric*
 774 *Sciences*, 73(4), 1667–1686. <https://doi.org/10.1175/JAS-D-14-0327.1>
- 775 Poulidis, A. P., Takemi, T., Iguchi, M., & Renfrew, I. A. (2017). Orographic effects on the
 776 transport and deposition of volcanic ash: A case study of Mount Sakurajima, Japan.
 777 *Journal of Geophysical Research: Atmospheres*, 122(17), 9332–9350.
 778 <https://doi.org/10.1002/2017JD026595>
- 779 Rampino, M. R., Self, S., & Fairbridge, R. W. (1979). Can Rapid Climatic Change Cause
 780 Volcanic Eruptions? *Science*, 206(4420), 826–829.
 781 <https://doi.org/10.1126/science.206.4420.826>
- 782 Robock, A. (2000). Volcanic eruptions and climate. *Reviews of Geophysics*, 38(2), 191–219.
 783 <https://doi.org/10.1029/1998RG000054>
- 784 Rolandi, G., Barrella, A. M., & Borrelli, A. (1993). The 1631 eruption of Vesuvius. *Journal of*
 785 *Volcanology and Geothermal Research*, 58(1), 183–201. [https://doi.org/10.1016/0377-0273\(93\)90107-3](https://doi.org/10.1016/0377-0273(93)90107-3)
- 787 Sanderson, R. W., Matoza, R. S., Haymon, R. M., Steidl, J. H., & Hegarty, P. (2018). Lahar
 788 detection using infrasound: Pilot experiment at Mount Adams, WA. *AGU Fall Meeting*
 789 *Abstracts*, 13. Retrieved from <http://adsabs.harvard.edu/abs/2018AGUFM.V13D0118S>
- 790 Scandone, R., Giacomelli, L., & Gasparini, P. (1993). Mount Vesuvius: 2000 years of
 791 volcanological observations. *Journal of Volcanology and Geothermal Research*, 58(1–4),
 792 5–25. [https://doi.org/10.1016/0377-0273\(93\)90099-D](https://doi.org/10.1016/0377-0273(93)90099-D)

- 793 Swindles, G. T., Watson, E. J., Savov, I. P., Lawson, I. T., Schmidt, A., Hooper, A., et al. (2017).
 794 Climatic control on Icelandic volcanic activity during the mid-Holocene. *Geology*, *46*(1),
 795 47–50. <https://doi.org/10.1130/G39633.1>
- 796 Taron, J., Elsworth, D., Thompson, G., & Voight, B. (2007). Mechanisms for rainfall-concurrent
 797 lava dome collapses at Soufrière Hills Volcano, 2000–2002. *Journal of Volcanology and*
 798 *Geothermal Research*, *160*(1–2), 195–209.
 799 <https://doi.org/10.1016/j.jvolgeores.2006.10.003>
- 800 Taylor, K. E., Stouffer, R. J., & Meehl, G. A. (2012). An Overview of CMIP5 and the
 801 Experiment Design. *Bulletin of the American Meteorological Society*, *93*(4), 485–498.
 802 <https://doi.org/10.1175/BAMS-D-11-00094.1>
- 803 Tebaldi, C., Hayhoe, K., Arblaster, J. M., & Meehl, G. A. (2006). Going to the Extremes.
 804 *Climatic Change*, *79*(3), 185–211. <https://doi.org/10.1007/s10584-006-9051-4>
- 805 Tormey, D. (2010). Managing the effects of accelerated glacial melting on volcanic collapse and
 806 debris flows: Planchon–Peteroa Volcano, Southern Andes. *Global and Planetary*
 807 *Change*, *74*(2), 82–90. <https://doi.org/10.1016/j.gloplacha.2010.08.003>
- 808 Towhata, I., Goto, S., Goto, S., Akima, T., Tanaka, J., Uchimura, T., et al. (2021). Mechanism
 809 and future risk of slope instability induced by extreme rainfall event in Izu Oshima
 810 Island, Japan. *Natural Hazards*, *105*(1), 501–530. [https://doi.org/10.1007/s11069-020-](https://doi.org/10.1007/s11069-020-04321-0)
 811 [04321-0](https://doi.org/10.1007/s11069-020-04321-0)
- 812 Violette, S., Marsily, G. D., Carbonnel, J. P., Goblet, P., Ledoux, E., Tijani, S. M., & Vouille, G.
 813 (2001). Can rainfall trigger volcanic eruptions? A mechanical stress model of an active
 814 volcano: ‘Piton de la Fournaise’, Reunion Island. *Terra Nova*, *13*(1), 18–24.
 815 <https://doi.org/10.1046/j.1365-3121.2001.00297.x>
- 816 Voight, B., Constantine, E. K., Siswamidjyo, S., & Torley, R. (2000). Historical eruptions of
 817 Merapi Volcano, Central Java, Indonesia, 1768–1998. *Journal of Volcanology and*
 818 *Geothermal Research*, *100*(1), 69–138. [https://doi.org/10.1016/S0377-0273\(00\)00134-7](https://doi.org/10.1016/S0377-0273(00)00134-7)
- 819 Yamasato, H., Kitagawa, S., & Komiya, M. (1998). Effect of rainfall on dacitic lava dome
 820 collapse at Unzen volcano, Japan. *Papers in Meteorology and Geophysics*, *48*(3), 73–78.
 821 <https://doi.org/10.2467/mripapers.48.73>
- 822 Zhou, C., Zelinka, M. D., Dessler, A. E., & Wang, M. (2021). Greater committed warming after
 823 accounting for the pattern effect. *Nature Climate Change*, *11*(2), 132–136.
 824 <https://doi.org/10.1038/s41558-020-00955-x>
- 825
 826
 827
 828
 829

830

831

832

833

834

835

836